academicJournals

Vol. 5(7), pp. 128-144, October 2013
DOI 10.5897/JMER2013.0262
ISSN 2141-2383 © 2013 Academic Journals
http://www.academicjournals.org/JMER

Journal of Mechanical Engineering Research

Full Length Research Paper

Study of effects of burner configuration and jet dynamics on characteristics of inversed diffusion flames

Hussien Zaky Barakat, Mohamed Refaat Salem, Abdelaziz Morgan and Hany Elsayed Saad*

Mechanical Power Department, Ain Shams University, Cairo, Egypt.

Accepted 6 September, 2013

The effect of the geometric parameters and jet dynamics of the port array inverse diffusion flame (IDF) burner on the flame characteristics were investigated experimentally using liquefied petroleum gas (LPG) fuel. The geometric parameters are the central air flow area, the fuel jets flow area, the number of the fuel jets and the radius of the pitch circle around which the fuel ports are arranged. The jet dynamics are the air and the fuel flow rates and their momentum flux. Three burners were used for this purpose. The analysis of the results of the IDF jet dynamics showed that two flame fronts formed in the entrainment zone of the IDF, one of them in the co-flowing jet formed by the fuel and the central air jet and the other is in the peripheral submerged jet formed by the fuel jets and the ambient air. Beyond the neck, the central air jet, the fuel jets and the two flame fronts flow as one flame torch. At high air, Reynolds number and low fuel Reynolds number, corresponding to the primary equivalence ratios near unity, the IDF produced by the burner of pitch circle radius 10 mm are short blue color sootless flames. As the air Reynolds number was gradually decreased to a low value corresponding to a primary equivalence ratio 4.5, the flame was changed to yellow diffusion flame with high soot concentrations. The results also showed that the flame characteristics were highly affected by the number of the fuel ports. The flame became more bluish and shorter as the number of the fuel ports increases to 36 ports.

Key words: Inverse diffusion flame (IDF), diffusion flame, burner configuration.

INTRODUCTION

Flames formed by combustion of gaseous fuels may take two forms: premixed flames or diffusion flames. Premixed flames occur when the fuel and the oxidizer are mixed upstream of the delivery to the combustion zone. Diffusion flames occur when the fuel and oxidizer are separately delivered to the combustion zone (Elmahalawy et al., 2002).

Due to their non-premixed nature, the normal diffusion flames have a wide flammability range even in turbulent states. But the high soot loading characteristic limits the application of these flames in domestic applications for which clean combustion is required. Premixed flames are cleaner and burn more intensely; but, the operating range is narrow due to the flash back or lift-off of the flame (Sze Lip Kit, 2007). These drawbacks of the premixed flames and the relatively small effective heating area of high temperature and safety requirement limited their applications in industrial application and impingement

*Corresponding author. E-mail: H_saad80@yahoo.com. Tel: +201000385638.

Abbreviations: IDF, Inverse diffusion flame; **CAP**, Circumferentially arranged ports; **NDF,** Normal diffusion flame.

heating.

IDF as a kind of diffusion flame with an inner air jet being surrounded by outer fuel jets in either confined or unconfined conditions shows no flashback, less soot loading than normal diffusion flame, low NOx and has a wide range of flammability (Salem, 2007). These features make the use of IDF burners feasible and are becoming of growing interest in industrial heating processes, but few studies have been performed using the IDF configuration compared to the normal diffusion flames literature.

The majority of the previous studies of the IDFs are concerned with the flame shape, height, temperature distribution, oxygen, carbon dioxide, and carbon monoxide concentrations as well as NOx and soot emissions. Wu et al. (1984) described a map of different IDF types against different combination of air jet and fuel jet velocities. The IDF reported by (Wu et al., 1984) is a blue bell shaped laminar flame attached to the air jet exit. At high overall equivalence ratio, an orange-yellow cap is developed upon the blue reaction zone. They also compared between the laminar normal diffusion flames (NDF) and IDFs. Huang et al. (1997) conducted similar research on the double concentric jets using a central air jet and an annular fuel jet. Takagi et al. (1996) studied experimentally and numerically the difference between normal and inverse laminar diffusion flame, using nitrogen diluted hydrogen fuel. Partridge et al. (1999) seemed to be the first to offer literature on the no formation characteristic of IDF.

Sze et al. (2006) carried out experiments to investigate the shape, height, temperature distribution, and NO*x* emission of two unconfined IDF, one with circumferentially arranged ports (CAP) and the other with co-axial (CoA) jets, both using LPG as fuel. They observed that, the entrainment zone can be observed only at high air Reynolds number larger than 2500. The CoA flame in most cases is similar to a diffusion flame. They also reported that, a negative pressure region is formed between the jets resulting in the flow of the fuel jets towards the central air jet within the entrainment zone. Sze et al. (2004) conducted experiments on IDF burning butane. The IDF has a central air jet surrounded by 12 circumferentially arranged fuel jets each 2.4 mm with center to center distance 11.5 mm similar to that used by (Sze et al., 2006). They investigated the temperature distribution, heat transfer characteristics, flame height, and species concentration of impinging IDF. They reported that the height of the entrainment zone increased slightly with increase in Re_{air} and Φ_o. They found that the IDF have two regions of maximum temperature around the flame centerline. The maximum temperature zone appears close to the top of the entrainment zone. Sze et al. (2006) concluded that the centerline oxygen concentrations in CAP flames decreased steeply with the flame height until reaching a minimum value as it is depleted by combustion and then increased due to the entrainment of atmospheric air into the flame tail where combustion has been almost completed. Dong et al. (2007) stated that seven IDF structures have been observed altogether. The experiments were carried out on an IDF burner as used by (Sze et al., 2004, 2006). They found that, fuel/air jet entrainment is a crucial factor determining the flow and flame structures of the concentric co-flowing IDF. Mikoski (2004) studied the flame structure and soot and carbon monoxide (CO) formation were studied in laminar co-flowing co-annular IDFs. (Choy et al., 2012), reports an experimental investigation of the pollutant emission and noise radiation characteristics of both open and impinging IDFs, produced by five burners of different air port diameter (d_{air}) and air-to-fuel spacing (S). The effects of d_{air}, S, overall equivalence ratio Φ_o and nozzle-to-plate spacing, H, on the pollutant emissions of CO and NOx and the noise radiation are examined. They concluded that, for each flame, the fuel jets are shifted towards and entrained into the air jet once they flow out of the fuel ports. This is because a low pressure zone was created around the root of the air jet due to its high velocity. They also concluded that as d_{air} increases, the pale blue outer layer overlapping the deep blue inner reaction cone changes its color, with more yellow-colors present in this layer. They stated that the reason is simply that at a fixed air flow rate, a smaller d_{air} results in a higher air jet velocity or Re, which enhances air/fuel mixing and promotes premixed combustion. Mikofski et al. (2007), studied the flame structure of laminar IDFs to gain an insight into soot formation and growth in under ventilated combustion. In the work of (Zhen et al., 2010), the thermal and emission characteristics of a swirl-stabilized turbulent IDF burning LPG were studied.

A study of the effect of the pitch circle distance, S, between the center of the air port and the center of the concentrically arranged fuel ports and the air jet Reynolds number as well at constant fuel flow rate, constant air and fuel jets discharge areas, constant fuel Reynolds number and constant jet velocity, constant number of the fuel ports was undertaken by Salem (2007). Four burners having 10, 15, 20 and 25 mm fuel ports pitch circle radii were used to investigate the effect of the pitch circle distance, S, on the flame characteristics. Each burner had 12 fuel ports with 2 mm diameter each. The 10 mm pitch circle radius burner gave the most favorable flame. He concluded that, the nature of the flow of the fuel and air jets in the CAP burners make their flame either of the IDF and NDF. At large center to center spacing or low air Reynolds number the flame becomes a normal diffusion one.

From the above studies, it is found that the IDFs characteristics are affected by the jet dynamics and the burner configuration. The jet dynamics are defined by the central air and the fuel jets momentum flux, which for any given burner determine the primary equivalence ratio (Φ_p), the fuel and the air jet Reynolds numbers. The

burner configuration parameters are the pitch circle distance, the number of the fuel ports as well as the fuel and the air flow areas. Moreover, no study has been performed on the number of the fuel ports and little study has been performed on the effect of the change of the pitch circle distance on the flame structure. Therefore, the present investigation is concerned with the theoretical and experimental study of the influence of the IDF burners geometry and the jets dynamics on the nature of the free jet flames from IDF burners of port array type. The development of the co-flowing and the submerged jet flows is discussed. The formation of a fuel-air mixture boundary layer in both types of jet flow and the associated flame fronts are presented. The ambient air entrained by the submerged jet, its role and magnitude are investigated. The effect of the number of the fuel jets, the variation of the air jet Reynolds number and consequently the primary equivalence ratio, on these characteristics is given while keeping both of the total fuel flow rate and the fuel jets velocity unchanged. The results of the set of burners whose pitch circle radius 10 mm are presented in this paper. Discussion of the results on the background of the theory of heat, momentum and mass transfer in jet flows to cast some light on the effect of the burner geometry and the jet dynamics on the characteristics of the IDFs is presented.

EXPERIMENTAL SETUP

The experimental setup is shown schematically in Figure 1. The burner consists of two parts, namely, the burner head which is made of stainless steel plate and the fuel chamber as shown in (Figure 2).

Gaseous fuel LPG, (60%C_4H_{10} and 40% C_3H_8 by volume) was fed into the gas burner from a 37 liter LPG bottle at a gauge pressure of (5000±100) pa, after passing through a pressure reducer valve fitted in the LPG bottle outlet. This valve is used to keep the outlet gaseous fuel pressure at 3000 pa. The feeding fuel line is equipped with a calibrated pressure gauge, 6000 pa maximum pressure and placed after the pressure reducer valve (Figure 1). A regulator valve is used to control the fuel flow rate. The fuel delivery line is constructed from a seamless pipe, 12 mm diameter whose end is connected to a calibrated fuel rotameter used to measure the fuel flow rate. Air is forced through a pipe of 15 mm inner diameter and 125 cm length into the IDF burner from a 1000 Liter size compressor tank (Figure 1). The IDF is effected by supplying the air to the burner through one central port. The air mass flow rate is measured using a calibrated rotameter. The gaseous fuel supplied to the burner issues from it through a number of equal diameter fuel ports. The fuel ports of each burner are equally spaced around the air port on the same pitch circle. The inlet temperature of the air and the fuel are measured by two pairs of calibrated thermocouples type J. The inlet measured temperatures were 28°C and 25°C respectively.

Three sets of IDF burners each of which consists of three different pitch circle radius were used. The distances, S, which are the pitch circle radii, are 10, 15 and 20 mm (Figure 3). The corresponding pitch circle diameters are 20, 30, and 40 mm. Each set consists of three IDF burners that have the same pitch circle radii, but the number of the fuel ports in the three burners are different being either 12, 24 or 36 fuel ports. The total fuel flow area, which is the summation of the area of all the ports of the burner, was the same for all of the burners regardless of the number of ports used. The air flow area in all the burners was unchanged as the air outlet port was the same for all burners at 6 mm as shown in Table 1. The total fuel flow area in this work was 1.25 times that of the air port. The fuel flow area was equal to that used by Salem (2007). The air flow area used by Salem (2007) is 1.36 times the area in this study.

In the present study, the fuel flow area was kept constant by decreasing the ports diameter if the number of ports was increased as shown in Table 1. The fuel ports were opened by a laser drilling machine.

The appearance of the IDF under different operating conditions was obtained using a digital camera with 12 Mega pixels, 50 frames per second imaging rate. The position of the camera relative to the flame was the same during all shots in order to keep the height and size scales the same for all shots.The flame temperature was measured using type S (Pt-Pt Rh 10%) thermocouples. The type S thermocouple wire diameter is 0.1 mm. The diameter of the ceramic tube in which the thermocouple wires were enclosed is 3 mm and its bead size is almost 200 µm to minimize flame disturbance during measurements. During the experiments, the thermocouple was aligned with the burner such that it can be moved in a 2-D space in order to obtain the flame temperature distribution in axial and radial directions. The thermocouple bead was aligned co-axially with the air jet centerline each time before measurement. The temperatures reported have been corrected for radiation loss with the method suggested by (Bradley and Matthews, 1968). The maximum temperature correction in this work was 144°C. The gas species concentration, on dry basis, is measured using flue-gas analyzer, model Land-Lancom III.

All tests are carried out with a fixed fuel flow rate 0.025 L/s (25×10^{-6} m^3/s). The fuel Reynolds number varied due to the decrease of the fuel ports diameter as their number was increased. The decrease of the fuel Reynolds number is limited, as it was 377, 266, 218 for the 12, 24, and 36 fuel ports respectively, compared to the change in the air jet Reynolds number which varied from 10446 to 4703 as shown in Tables 2. Four experiments have been carried out on each of the burner groups at four primary equivalence ratios of 0.9, 1, 1.2, and 2 corresponding to air jet Reynolds number 10446, 9379, 7831 and 4703 respectively. Other experiments were carried as needed to investigate the flame characteristics at operating conditions outside the range of the air or the fuel flow rates.

As the fuel flow rate during these tests was kept constant, the change in the air Reynolds number necessarily leads to a corresponding variation of the primary equivalence ratio Φ_p. In this case any change of the flame characteristics as the central air Reynolds number was varied is the combined effect of the variation of both of the central air Reynolds number and the primary equivalence ratio, Φ_p.

The base case, selected to present the subject of this paper which is concerned with the flame nature, the co-flowing and submerged fuel-air mixture boundary layers, the flame fronts and the entrained ambient air at different number of the fuel ports, is the results obtained by the three burners whose pitch circle is 10 mm. Reference to results obtained by other burners is given when it is necessary.

To ensure the repeatability, each run of experiments was conducted two times and the averaged values are reported and employed to perform the error analysis. The error analysis was performed with the method of Kline and McClintock (1953). The precision of all flame height measurements was ±0.5 mm, and the precision in air flow rate measurements was ±10%. With 95% confidence level, the minimum and maximum uncertainties in the flame temperature measurements are 2.6% and 10.4%, respectively.

The minimum and maximum uncertainties of CO measurement are 2.1 and 9.5%, respectively. The uncertainty of the NO

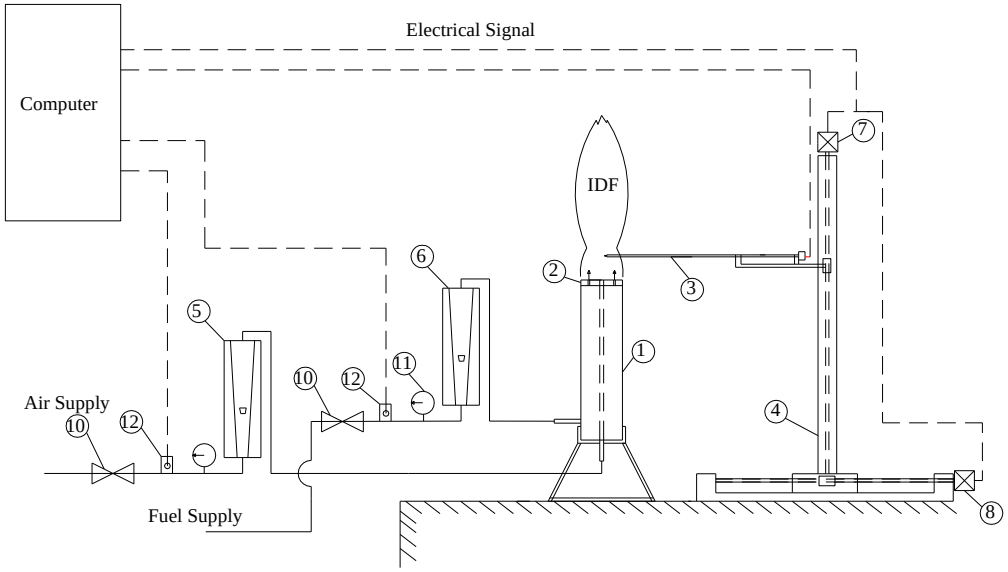

1	**Burner**	4	**2-D Thermocouple Positioner**	7	**Stepper Motor**	10	**Control Valve** **Pressure gauge**
2	Burner Head (Cap)	5	**Air Rotameter**	8	**Stepper Motor**	11	**Thermoucouple**
3	**Thermocouple Type S**	6	**Fuel Rotameter**	9	**Stepper Motor**	12	

Figure 1. Schematic of experimental set up.

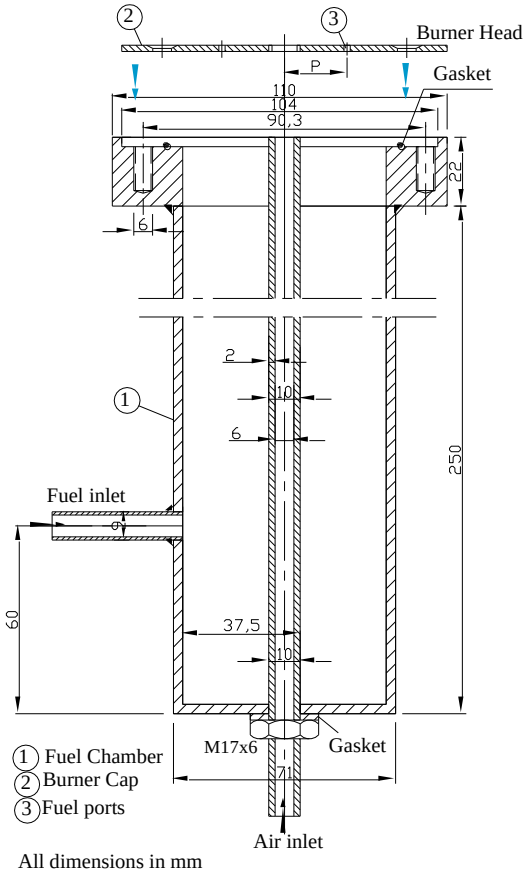

Figure 2. The burner.

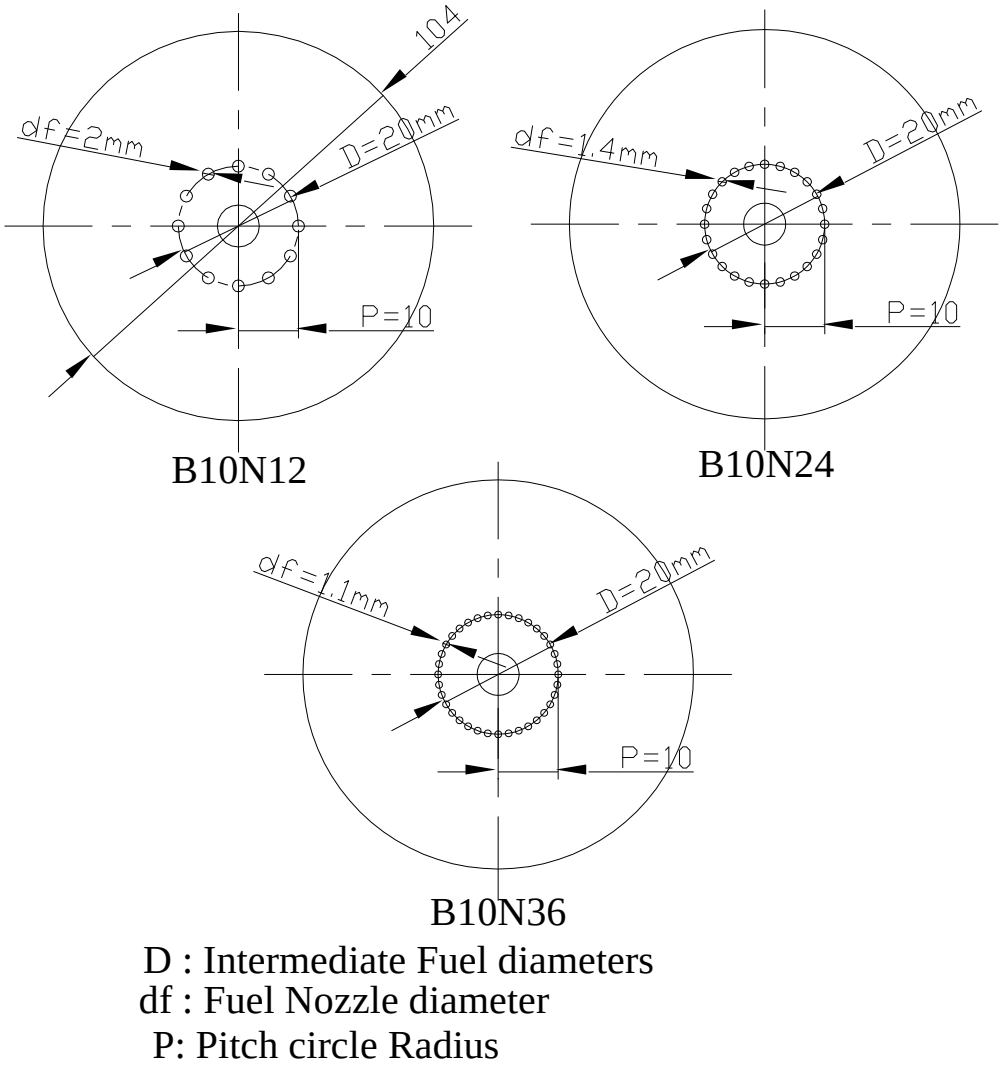

Figure 3. The burner cap group.

measurement ranges from 2.3 to 12.3%. The minimum uncertainties of CO_2 and O_2 are 1.1 and 1.3%, respectively, while their maximum uncertainties are 8.3 and 9.2%, respectively.

RESULTS AND DISCUSSION

Relationship between burner design parameters and jet dynamics

The influence of the burner design parameters on the value of the Reynolds number is examined having in mind that the value of the Reynolds number, Re, can be written in the following form,

$$\mathrm{Re} = \frac{4\overset{o}{m}}{\pi\mu d} \quad (1)$$

Where $\overset{o}{m}$, is the mass flow rate of the fluid, μ is the fluid viscosity which measured at the ambient temperature and d is the fluid exit port inner diameter; the fluid being either the fuel or the central air. The value of the Reynolds number, as given by Equation 1, can be changed to a higher value for the same fluid by decreasing the diameter while keeping the mass flow rate at the same value or increasing the mass flow rate while keeping the fluid port diameter without change. The decrease of the Reynolds number can be achieved in a similar manner. The effect of the variation of the Reynolds number on the jet momentum flux and on the flame characteristics such as the flame structure, its temperature distribution and the concentration of the species of combustion will not be the same in both cases, even if the value of the Reynolds number is the same in

Table 1. Dimensions and symbols of the IDF nine burner heads.

Burner group	Symbol	Fuel diameter, d_f (mm)	Air jet diameter, d_a, (mm)	Pitch circle radius, P (mm)	No. of fuel jets (N_f)	Total fuel jets area$\times10^{-3}$ (m^2)	Air jet area$\times10^{-3}$ (m^2)
	B20N12	2	6	20	12	0.03768	0.02826
Group 1	B15N12	2	6	15	12	0.03768	0.02826
	B10N12	2	6	10	12	0.03768	0.02826
	B20N24	1.4	6	20	24	0.03768	0.02826
Group 2	B15N24	1.4	6	15	24	0.03768	0.02826
	B10N24	1.4	6	10	24	0.03768	0.02826
	B20N36	1.1	6	20	36	0.03768	0.02826
Group 3	B15N36	1.1	6	15	36	0.03768	0.02826
	B10N36	1.1	6	10	36	0.03768	0.02826

Table 2. Conditions of experiments.

Primary equivalence ratio (Φ)	Total fuel flow rate (L/min)	Air flow rate (L/min)	Fuel jet velocity (m/s)	Air jet velocity (m/s)	Air Reynolds number (Re_{air})	(Air momentum flux)/(Fuel momentum flux)=$\rho_{air}V^2_{air}/\rho_{fuel}V^2_{fuel}$	Burner group	Fuel Reynolds number (Re_{fuel})
0.9	1.5	46.98	0.66	27.7	10446	964	Group 1	377
1	1.5	42.18	0.66	24.8	9379	777	Group 2	266
1.2	1.5	35.22	0.66	20.7	7831	542	Group 3	218
2	1.5	21.15	0.66	12.4	4702	195		

both cases. Similarly the value of the primary equivalence ratio,Φ_p, may be varied to take a particular value by varying the fuel flow rate, by changing the central air flow rate or by the variation of each of them. In this case also, the nature of the flame in each case will not be the same.

The distance between the centerline of the central air jet and the centerline of the peripherally arranged fuel ports, S, as well as the number of the fuel ports, N_f, exert an influential effect on the characteristics of the IDF flame through their influence on the momentum and mass transport between the air and the fuel jets and on the peripheral surface area of the fuel jets in contact with both of the central air jet and the ambient air as well. The lower pitch circle distance, S, allows better entrainment and mixing of the co-flowing air and the fuel jets, while the increase of the fuel jets peripheral area increases the rate of the central air-fuel mixing. In this case also, better mixing of the entrained ambient air is achieved.

The above discussions clearly show that the burner construction, the air and the fuel flow rates, their momentum flux and their Reynolds numbers are strongly interrelated. These parameters together determine what type of flame that would be produced under any particular set of burner configuration and fuel and air flow rates. For these reasons, the influence of the CAP burner design parameters, as well as the fuel and the central air Reynolds numbers and the primary equivalence ratio, Φ_p, on the nature of the IDF flames, should be examined on the basics of the currently well developed theory of the dynamics of jet flows. Such an analysis is necessary because the IDF flames encompass, in the same time, two distinic types of jets, mainly the co-flowing jet stream and the submerged jet one as discussed below. A flame front is formed at the air-fuel interfacial surface of each jet in the entrainment zone; a feature which the normal diffusion flames, NDF, do not possess.

Co-flowing central air and fuel jets

The central air jet and each of the fuel jets at their plane of emergence from the burner top surface are separated by a distance, d_s, which is equal to the center to center distance, S, minus half the sum of the air jet and the fuel jet exit diameters.

$$d_s = S - (d_{air} + d_{fuel}) / 2 \quad (2)$$

As the two jets get out from the ports, they immediately transversally expand. After a very short distance from the

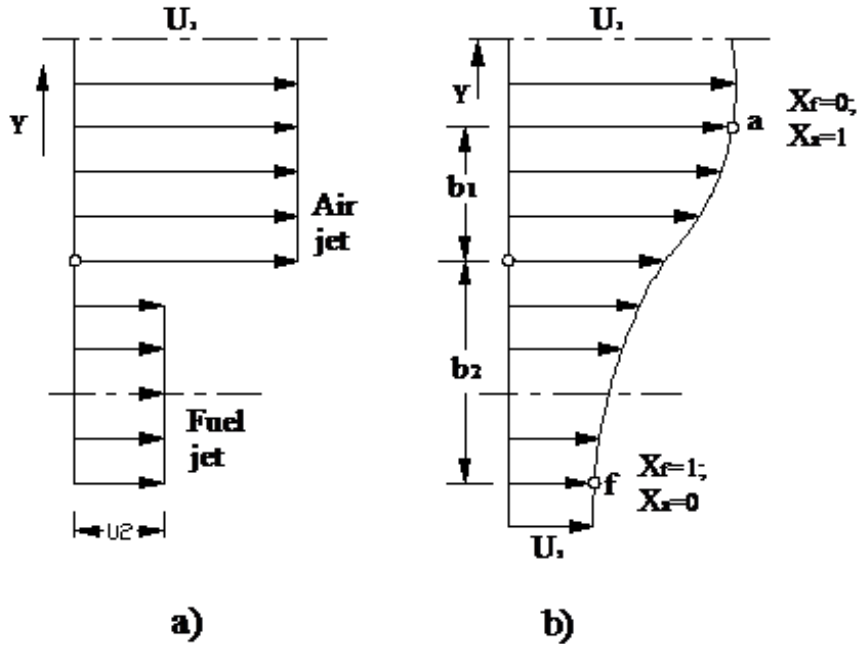

Figure 4. The velocity distribution and the air and the fuel concentrations, x_a&x_f of the co-flowing boundary layer; a) initial pattern, b) pattern an instant later.

plane of emergence the two jets adjoin and flow in the downstream direction or along the jet path, forming a co-flowing jet (Schilichting,1960) and (Abramovich, 1963). As the two jets emerge in the same direction at two different velocities, an unstable surface having a discontinuity in the velocity is formed at the boundary of the two jets. This interfacial instability gives rise to the formation of eddies that move randomly transversally and along the flow causing high momentum exchange between the two co-flowing streams that leads to smoothening of the velocity. Eddies formation continues downstream or upward with the flow direction beyond the point at which the two jets merge. This situation gives rise to a continuing turbulent exchange of momentum, mass and heat transfer at the interface of the two streams. Such a case leads to the formation of a fuel-air mixture boundary layer of finite thickness at the interface of the air and fuel streams. This boundary layer is often termed the shear layer.

The co-flowing boundary layer thickness at the point of merging is zero and it increases as the jets move upward the point of merging. In this work, this layer will be referred to it briefly as the co-flowing or the inner boundary layer. Figure 4 depicts the velocity distribution in this case, but the boundary layer thickness will be much less than that of Figure 4. Point (a) identifies the inner that is, the air side edge of this boundary layer, while point (f) identifies the outer edge that is, the fuel side edge of the co-flowing boundary layer. The transversal distances b1 and b2 in Figure 4b represent the portion of the boundary layer in the air jet and the fuel jets sides respectively.

At the initial region of the co-flowing boundary layer, the transport of the air into the developing co-flowing admixture boundary layer is by turbulent mass transfer. The laminar as well as the turbulent boundary layer equations for momentum, energy and mass transport, for which similar solutions exists, apply for this case and gave good results for the dimensionless distribution of each of the temperature and concentration in jet flow of gaseous mixtures.

The air concentration in the fuel stream side of the boundary layer is not transversally or axially uniform and the fuel concentration in the air side of it is also as such. The boundary conditions shown in Figure 4b for the concentration of the fuel and the air at points (a) and (f) of the boundary layer imply that the fuel and the air concentrations in the air-fuel mixture boundary layer are mirror images. The fuel-air mixture in the boundary layer is lean in the air jet vicinity, while it is rich in the fuel jet neighborhood. Therefore, somewhere in the boundary layer there will exist a region in the co-flowing boundary layer in which a combustible air-fuel mixture is formed. This region extends between the central air port exit and that of the fuel jets ports. Once a sufficiently preheated combustible mixture is formed anywhere in this boundary layer, combustion takes place at this location in the co-flowing jet boundary layer.

Figures 5a, b, c) show the radial temperature distribution at different flame heights from the burner rim for the B10N12 burner at different primary equivalence ratios, Φ_p. The thick arrow at the bottom of each figure

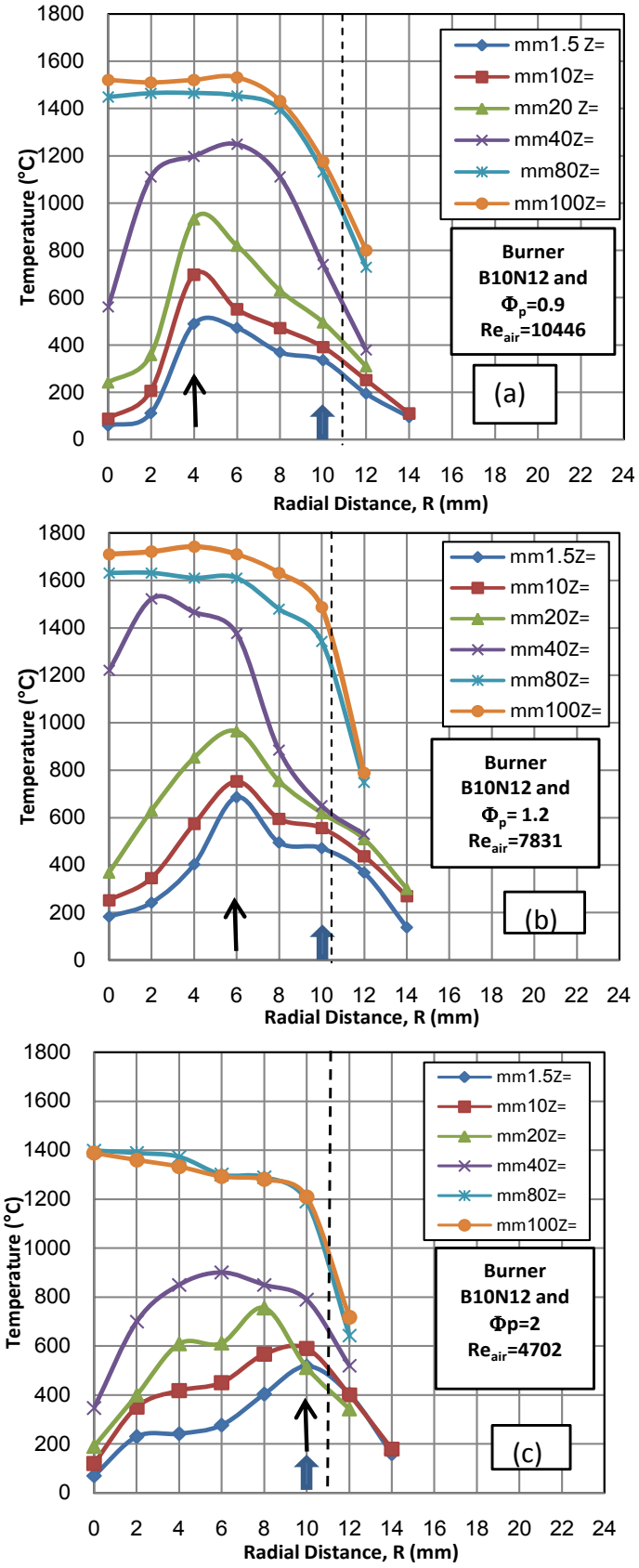

Figure 5. Radial temperature distribution in IDF at different vertical distances.

refers to the position of the fuel jet ports centerline. The dotted vertical line represents the ambient air side edge of the fuel port. In the analysis of the IDF centerline temperature distribution, it was found that for a small vertical distance from the burner tip that equals about 20 mm, the flame temperature is lowest at the flame centerline. Beyond this height, the temperature increased with the height to reach a peak value in the reaction zone before the flame end, and then it begins to decrease as the post flame zone is approached. These figures show the presence of high temperature zones in the distance between the central air port and the fuel jet ports at equivalence ratios 0.9, 1.2 and 2, at the low distances near the burner tip from Z=1.5 mm up to Z=20 mm which represent the entrainment zone. The high temperature zone is 4 mm from the central air jet for the high jet momentum flux case at the Reynolds number 10446 corresponding to Φ_p=0.9 as shown in Figure 5a referred by the thin arrow. This is due when the interference between the air and fuel jets becomes strong enough, at high air Reynolds number, the fuel jets will be sucked to the co-flowing inner zone formed near the air jet. This zone shifts to almost half way the distance between the central air jet and the fuel jets at radial distance 6 mm for the moderate Reynolds number, 7831 corresponding to Φ_p=1.2, as shown in Figure 5b. It is moved nearer to the fuel jets when the interference is weak, at low air Reynolds number, 4702, corresponding to Φ_p=2, the air and fuel jets develop separately with each behaving as a single jet, as shown in Figure 5c. As the flame height increased over Z ≥ 20 mm, a gradual heating up of the air core takes place. This heating up continues in the upward direction and the centerline flame temperature increases, as shown in (Figures 5a, b, c), from the flame height about Z=40 mm. At this flame height, the maximum radial flame temperature is close to the air jet centerline.

The lower heat release rate (Figure 5) in the central air side of the co-flowing jet, which exists to the left of the point of the highest temperatures, is due to the lower fuel concentration as the air port is approached, the lower mixture temperature as well as the presence of more air there which causes an additional decrease of the jet temperature. In fact, for the system of multiple jets, the flow field is very complicated.

The submerged fuel-ambient air jet

In the mean time, the fuel jets which emerge in the stagnant ambient air form free submerged jets. The momentum efflux from the fuel ports causes a pressure drop around the fuel jets. This pressure drop can be evaluated considering that the stagnant ambient air pressure away from the jets is p_∞, that of the entrained air at the fuel jet emergence is p, and the entrained ambient air as it adjoins the fuel jets, by virtue of the nonslip condition, moves at the fuel jet velocity, then:

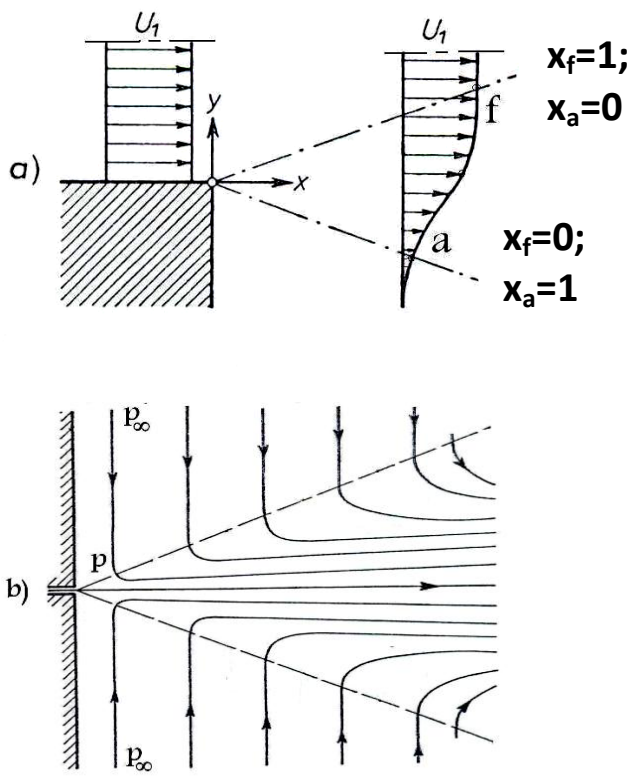

Figure 6. a) The submerged jet velocity and concentration boundary layer, b) The stream-lines in a circular free jet.

$$\Delta p = p_\infty - p = \rho_{air} v_{fuel}^2 / 2 \quad (3)$$

Where, ρ_{air} and v_{fuel} are the air density and the fuel velocity respectively. As a result of this pressure drop the ambient air is drawn to the base of the submerged jets and is entrained with them due to the momentum exchange caused by the turbulent friction at the interfacial surface between the submerged jets and the ambient air. The submerged jets also expand as they flow upward or downstream continually entraining ambient air. Due to this entrained ambient air, the mass of the jets increases as the jets spread and flow upward or downstream. Turbulent mixing and turbulent mass transfer at the interface of the submerged jet and the ambient air lead to the formation of another air-fuel mixture boundary layer in which the concentration of both of the species vary transversally and upward or downstream-wise. This boundary layer differs from that second flame front mentioned by Abramovich (1963), as each of them is formed by a different driving potential.

Figure 6 represents an enlarged orientation for the velocity distribution in the initial region in the entrainment zone of the developing submerged air-fuel mixture boundary layer. Point (a) on this figure represents the air-side end of this boundary layer, while point (f) is its fuel - side end. In this case also, the dimensionless velocity distribution is given by a similarity solution. At the exit of the fuel jets and as the fuel-air mixture boundary layer is developing, the dimensionless concentrations of both of the air and the fuel in the submerged boundary layer mixture will show also an analogous similarity solution as that of the velocity in this boundary layer. The strength of the air-fuel mixture in this boundary layer depends upon the fuel jet momentum flux and the scale of turbulence there. In the present case the rate of burning will be much lower than in the co-flowing boundary layer because the fuel jets velocity and consequently its momentum flux are low.

The temperature distribution in Figure 5 also shows that, although of the quenching effect of the entrained ambient air, the temperature at the center of the fuel jets and also that at the ambient-air-side of the fuel jets are much higher than at the center of the air jet. As mentioned above the rate of fuel burning at this flame front and consequently the rate of heat release there is much less than that of the co-flowing boundary layer. Therefore the temperature in this region will not be as high as that midway between the fuel and the central air jets. Such a high temperature in the ambient air side of the flame, which also extends some millimeters to the right of the fuel jet port into the ambient air region, is due to the existence of the flame front formed by the fuel-air mixture boundary layer of the submerged fuel-ambient air jet.

Formation of the flame fronts

In both of the co-flowing and the submerged boundary layers, the steady state concentration of the fuel is maximum at the fuel-side end of the boundary layers that is, at point (f) (Figure 4 and 6), and it is minimum at the air-side end of the boundary layer at point (a) in the same figures. As mentioned before, analogy between the dimensionless concentrations of the air and the fuel in the fuel-air mixture exists in the initial entrainment region of the jet during the stage of the boundary layers formation. The dimensionless distribution of the air concentration, as the boundary conditions at points (a) and (f) in Figure 4 and 6 imply, is nearly the inverse of that of the fuel, a mirror image form.

This reveals that somewhere in the two co-flowing and the submerged boundary layers of the fuel-air mixture, two circumferential zones having combustible mixtures will be formed; one of them is in the co-flowing boundary layer at the interfacial surface between the two co-flowing jets and the second is in the submerged boundary layer. This means that at least two flame fronts will exist in such IDF flames. As a sufficiently heated combustible mixture in any of these boundary layers is formed, burning of the fuel-air mixture takes place there.

Each of the air-fuel mixture boundary layers consists of two regions. A region in which the reactants are preheated by the turbulent eddies of the hot combustion

products to almost the combustion temperature and where a negligible amount of the reactants are burned. The rest of the air-fuel boundary layer is a much thinner reaction region in which the bulk of the combustible mixture is burned. The latter zone is the flame front of very thin thickness.

Because of the presence of the center to center distance, d_s, given by equation 2, between the air and the fuel jets, the formation of the outer fuel-air boundary layer starts before the co-flowing fuel-air mixture boundary layer regardless of its relative strength, which depends upon the fuel jets momentum flux. The time lag between them is definitely very short due to the narrow separating distance between the co-flowing jets and the short distance after which the two co-flowing jets merge as they immediately expand.

In the steady state, the initiation of combustion in this zone may precede that at the inner fuel-air mixture boundary layer of the co-flowing jets, if the fuel jet momentum flux is quite high to produce a combustible mixture in the submerged boundary layer, regardless of its strength, before that in the co-flowing boundary layer.

The two photographs shown in Figure 7 for the IDF entrainment zone produced at an air jet Reynolds number 13341 and 17788, with two relatively high fuel jets Reynolds numbers of 1256 and primary equivalence ratios, Φ_p=2.34 and 1.78 depict clearly these flame fronts, an inner co-flowing flame front enclosing a cold air core and the submerged flame front which extends in the ambient air beyond the fuel jet exit ports. These flame fronts merge together at the flame neck as shown in the figure.

The postulation presented above regarding the formation of two flame fronts, one of them in the submerged boundary layer at the outer envelope of the fuel jets and the other one in the co-flowing air-fuel mixture boundary layer at the central air-fuel interface, shows up in the measured temperature distribution given in Figure 5. This figure shows the temperatures at the outer boundary layer of the flame near the flame base in the entrainment zone about 300 to 550°C where the submerged boundary layer of the jet is formed. A high temperature zone in between the central air port and the fuel jets exists also in this figure where the temperature is about 700°C, while the temperature at the center of the port of the central air jet at the base of the flame, Z~1.5 mm, is much lower than the flame temperatures at the two mentioned zones. This observation confirms the presence of the two flame fronts.

Effect of the number of fuel jets

Among the burner design parameters that affect the characteristics of the inversed diffusion flames is the number of the fuel ports. As the number of the fuel jets is changed from N_{f1} to a higher number N_{f2}, while the total fuel ports area, the total mass flow rate of the fuel and the fuel jet velocity are all kept constant, the total fuel momentum and the fuel momentum flux remain also the same. In this case, the total circumferential surface area of the fuel jets at the emergence of the jets from the fuel ports per unit height of the flame will increase as the number of the fuel ports increases.

In this case if the interfacial surface area per unit length of the height of the higher number of the fuel ports is A_{fN2} and that of the lower number of the fuel ports is A_{fN1}, the ratio (A_{fN2}/A_{fN1}) will be higher than unity and it is given by:

$$(A_{fN2}/A_{fN1}) = \sqrt{N_{F2} / N_{f1}} \quad (4)$$

In this case the interfacial surface area between the fuel jets and the central air jet as well as that between the fuel jets and the ambient air, at which the jets exchange momentum, heat and mass with each of the central and ambient air, becomes larger as the number of the fuel jets increases. As a consequence the fuel-air mixture boundary layers, that develop as described before at the fuel-central air interface and at that of the fuel-ambient air, become larger. As a result the formation of the combustible mixture zones becomes time-wise higher and area wise larger.

The inter-air-fuel jets surfaces at the jets emergence at which the discontinuity in the jets velocity exists as described before also increase, giving rise to more interfacial instabilities of the flow. The increase of the region of instability of the flow leads to an increase in the turbulent eddies there, which once they are formed they move down stream that is, along the flame height, and decay. The agitation caused by these eddies as they form, move and decay randomly enhances the turbulent momentum, heat and mass transport in the entrainment zone. The ultimate effect of such flow dynamics is a high rate of formation of combustible well mixed fuel-air mixtures of higher burning rates.

For a particular burner, these effects take place in the IDFs at different scales depending upon the fuel and the air momentum fluxes, their ratio, the value of the pitch circle radii, the number of the fuel ports and the flow areas of the central air and fuel ports.

The influence of the number of the fuel ports on the flame color is noticed (Figures 8 and 9).

The flame colors produced by the high number of the fuel jets 24 and 36 that have lower fuel Reynolds numbers of 266 and 218 respectively, which are shown in (Figures 8 and 9), at two different equivalence ratios 0.9 and 1.2 are of more-dark blue ones than that of the flames produced by the burner that has the lower jets, B10N12, located on the same pitch circle radius of 10 mm, although the fuel jet Reynolds number of the 12 ports burner is higher. This is a result of the better mixing and the rapid formation of combustible fuel-air mixtures of higher burning rates by the larger number of the fuel ports

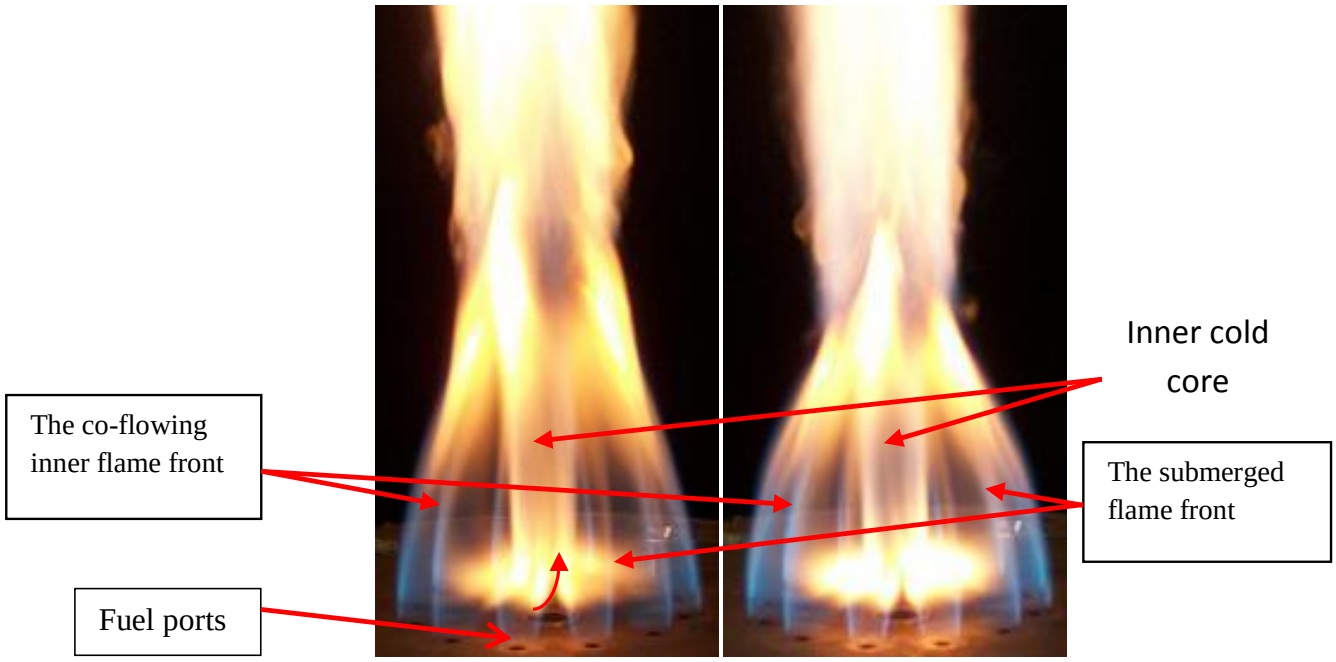

Figure 7. Photos for burner B20N12 at constant fuel flow rate 0.083 L/s of two air flow rates showing the two flame fronts and the cold core.

(a) (b) (c)
Re_{fuel}=377 Re_{fuel}=266 Re_{fuel}=218
B10N12, B10N24, B10N36

Figure 8. Effect of the number of fuel ports at Re_{air}=10466 orΦ_p =0.9 and burner B10N12, B10N24 and B10N36.

B10N12 B10N24 B10N36
N_f=12, N_f=24, N_f=36

Figure 9. Effect of the number of fuel ports on the Flame configuration at air Reynolds Number 7831 (Φ_p=1.2) for burner B10.

discussed above.

The presented experiments showed that a large number of the fuel jets issuing from smaller diameter ports are more efficient than a lower number of fuel jets of larger diameters located at the same pitch circle having a high Reynolds number from which the fuel emerges at the same fuel total flow rate and the same velocity.

The 12 ports flame in Figure 8a is higher and thicker than the 24 port flame of Figure 8b and both of them are longer and thicker than the flame produced by the 36 ports burner. This phenomenon indicates also that the larger number of the fuel ports results in higher burning rates that consume the gaseous fuel at higher rates producing shorter and thinner flames.

(a) (b) (c)

B10N12, B10N24, B10N36

Figure 10. Effect of the number of fuel ports at Re_{air}=3762 and Φ_p =2.5.

(a) (b) (c)

B10N12, B10N24, B10N36

Figure 11. Effect of the number of fuel ports at Re_{air}=2681 and Φ_p =3.5.

Effect of each of the air and fuel jet momentum flux and their Reynolds numbers on the nature of the flame

If the central air jet momentum flux is quite high and the fuel jet momentum flux is low, which is the case in the present work, the produced flame will be an IDF one having a flame neck which is a characteristic feature of these flames. The flames shown in Figure 8 and 9 typify these flames. These figures represent the IDFs at high air Reynolds numbers obtained from the burners B10N12, B10N24 and B10N36 respectively. The air Reynolds number in these flames is a high value of 10466 and 7831, while the fuel Reynolds numbers are low and equal 377, 266 and 218, and the primary equivalence ratios for these flames are 0.9 and 1.2. The fuel jet outlet velocity and the fuel mass flow rate are the same as the total fuel jets area of the flames in Figure 8 and 9 is the same. The flame color in the figures except that of the left flame in Figure 9 is blue and sootless indicating complete combustion in these cases at such a high air Reynolds number the turbulent momentum and mass transfer cause the formation of strong well mixed fuel-air mixture co-flowing boundary layer of higher burning rate. In this case the produced flame is an IDF.

This type of the IDF continued to form as the central air mass flow was decreased and consequently the air Reynolds number is decreased, while the primary equivalence ratio, Φ_p, increased until a low Reynolds number of 2081 was reached. In this case, the flame color continued changing from being bluish soot free at the high air Reynolds number to become yellow sooty longer flame that lost appearance of the IDFs at the low airr number or high primary equivalence ratios Φ_p=4.5. Figures 10 and 11 which are obtained at Re_{air}=3762 and 2681 respectively and corresponding to a primary equivalence ratio 2.5 and 3.5 represent this mode of the flame variation.

If the momentum of the two jets is low, a yellow sooty neckless flame NDF, is formed as that produced by the low momentum free jet diffusion flames. The IDF in this case may retain, by its definition, its name but looses the shape, the structure and the characteristics of the IDF flames and takes the appearance of a NDF. Figure 12

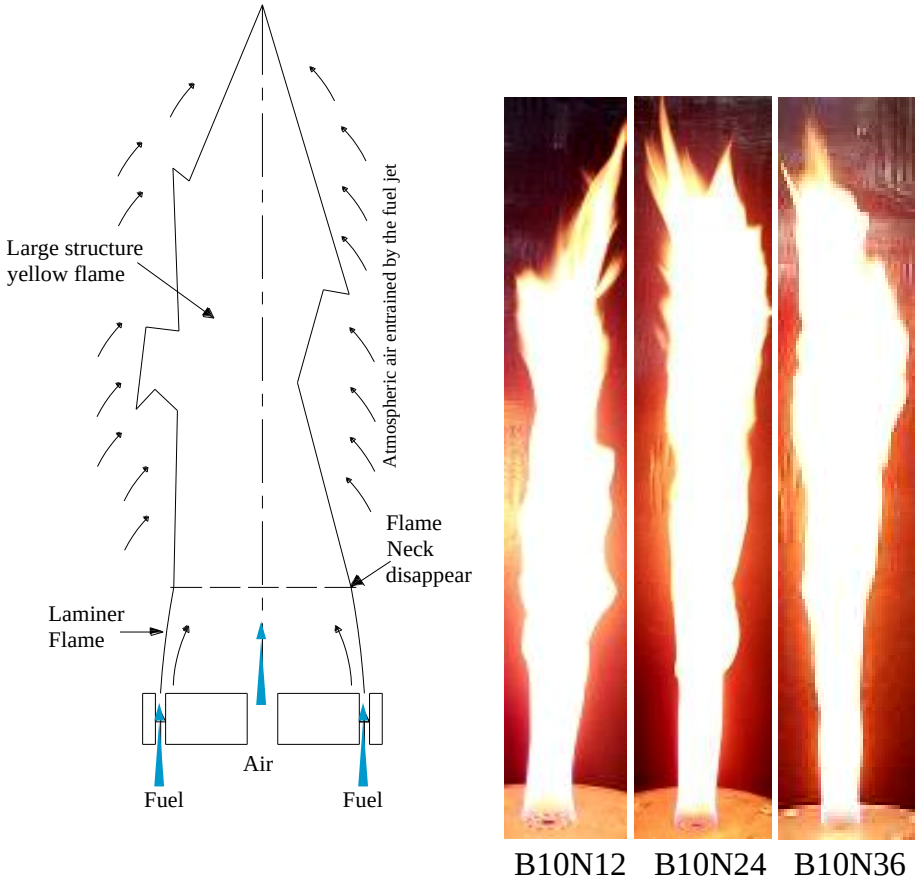

Figure 12. Schematic drawing and photos to show the diffusion flame at Re_{air}=2081, Φ_p =4.5, for burners B10N12, B10N24, and B10N36.

shows a schematic sketch for this case. The photos in this figure, were obtained by gradually decreasing the central air jet mass flow rate until this flame was formed at a low air Reynolds number, 2081, a fuel Reynolds number, 218 and a corresponding high primary equivalence ratio Φ_p =4.5, depict clearly such a NDF. Such NDFs at these Reynolds number levels took place at pitch circle radius 10 mm for all fuel jet numbers, 12, 24 and 36.

The flame neck

As the central air jet issues from its port at the high rate of momentum flux as in the high Reynolds number range of the present work, a pressure drop in the zone around the air jet, superimposed upon that created by the fuel jets, will take place. This pressure drop is much higher relative to that caused by the fuel jets because of the high air jet momentum flux compared to that of the fuel jets.

The ratio of the air jet momentum flux to the momentum flux of the fuel jet in this work varies from ~ 195 at the lowest air Reynolds number 4702 to ~964 at the highest air Reynolds number ~10446 as shown in Tables 2. According to Equation 3, the pressure drop caused by the issuing central air jet is 964 times that created by the fuel jets at the highest air Reynolds number 10466 to 195 times that of the fuel jets at the low air Reynolds number 4702.

Under these conditions a negative pressure gradient exists between the fuel jets and the central air jet; the pressure in the vicinity of the central air jet outlet is the lowest. As a result the fuel streams decline towards the central air jet as represented by the warped stream lines of the fuel jets in Figure 13.

The fuel is therefore drafted to tang with the air jet forming the entrainment zone which ends with the inverted bowel–shaped flame base. A neck of the least cross sectional area is formed as the fuel and the air jets completely tang. The distance at which the two jets tang will be shorter as the air jet momentum flux increases and vice verse. During this process mixing of the central air and the fuel takes place. The extent of this mixing depends upon the geometry of the burner and the jet dynamics. Beyond the neck zone the two jets merge forming a single plume. After merging at the neck, the

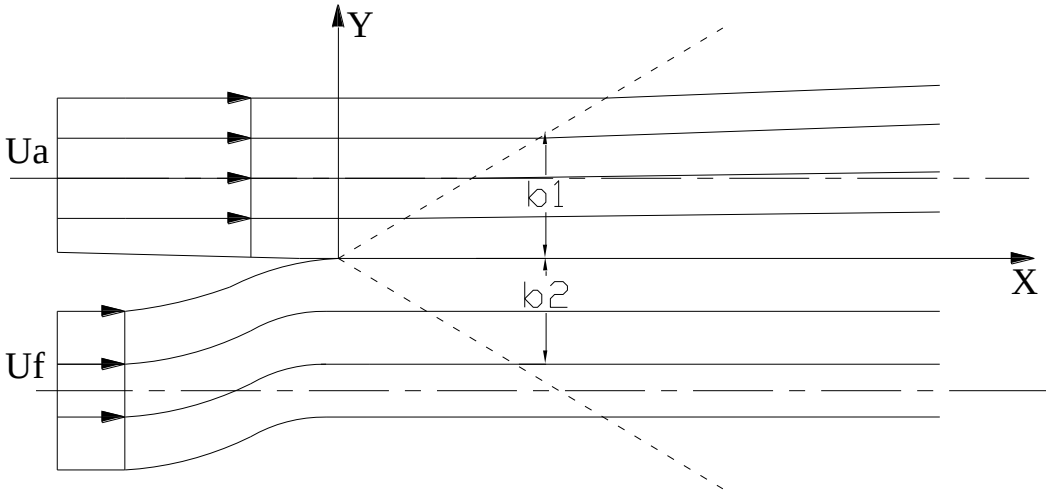

Figure 13. Streamlines in the neighborhood of the boundary layer of initial region of the jet.

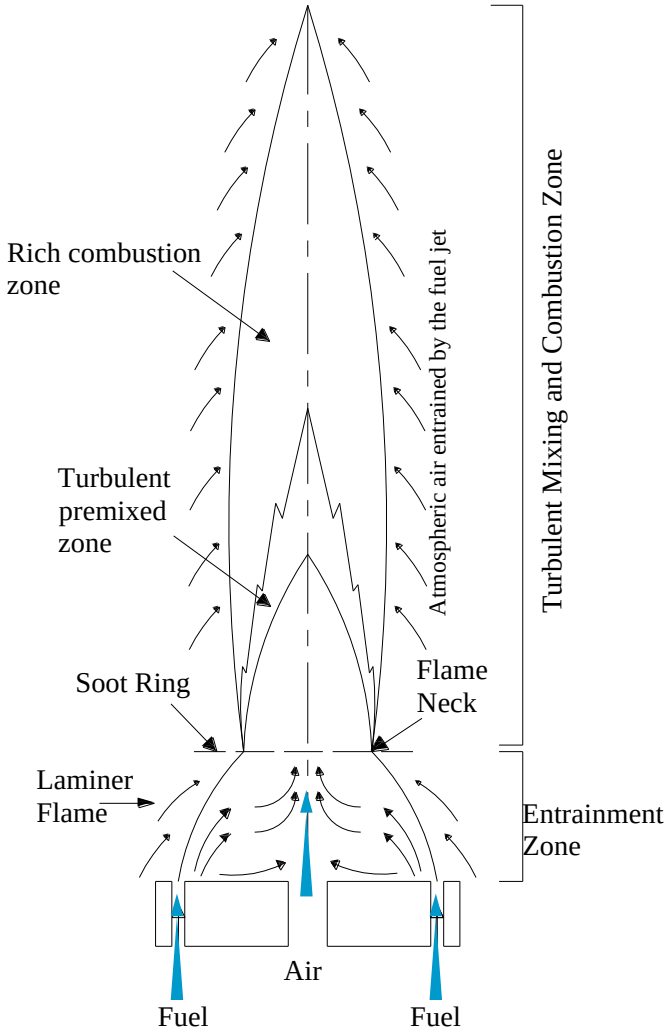

Figure 14. Schematic drawing showing a general structure of the IDF shape.

flame expands transversally as it flows upward and becomes of larger diameter to some of the flame height. After then the flame size begins to diminish until eventually disappears when the fuel is wholly consumed. Therefore the shape of the flame takes the form shown in Figure 14.

Effect of the number of fuel ports, central air jet Reynolds number and primary equivalence ratio on the flame neck

The inverted-bowell shaped necked entrainment zone appears in the photographs of the high air Reynolds number 10466 or at the primary equivalence ratio, Φ_p=0.9, flames (Figure 8). The formation of the flame neck for the three burners B10N12, B10N24 and B10N36 at the high and medium values, in this investigation, of the air Reynolds number of 9739 and 7831, the corresponding primary equivalence ratios are 1 and 1.2 is presented in Figure 15, while that formed at the lower Reynolds number 4702 and a higher primary equivalence ratio Φp=2 is shown in Figure 16.

The figures for the flame entrainment zone given in Figure 15 and those given in Figure 16 show a blue color flame in the bottom portion of the entrainment zone followed by a yellow color flame that extends to the neck. The effect of the number of the fuel ports as well as the air Reynolds number and the associated primary equivalence ratio, Φ_p, on the shape, size and color of the flame in the entrainment zone is demonstrated in Figures 15 and 16. The yellow color on the top portion of the photos in Figure 15 at the higher Reynolds number 9379 and Φ_p=1 occupies smaller area compared to the yellow area on the neck of the flames at the intermediate Reynolds number 7831 and Φ_p=1.2 shown in Figure 16.

Re_{air}=9379

B10N12(Φ_p=1) B10N24 (Φ_p=1) B10N36 (Φ_p=1)

Re_{air}=7831

B10N12 (Φ_p=1.2) B10N24 (Φ_p=1.2) B10N36 (Φ_p =1.2)

Figure 15. Photos showing the entrainment zone of IDF for three burners having pitch circle radius 10mm, and different number of the fuel jets at Φ_p= 1 and 1.2.

Re_{air}=4072

B10N12 (Φ_p =2) B10N24(Φ_p =2) B10N36 (Φ_p =2)

Figure 16. Photos showing the entrainment zone of IDF for three burners having pitch circle radius 10 mm, and different number of the fuel jets at Φ_p= 2.

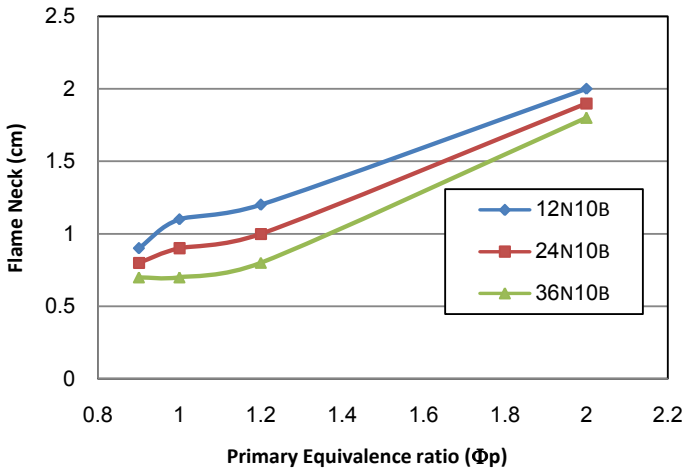

Figure 17. The entrainment zone height for burner B10 at number of the fuel ports 12, 24 and 36.

The photos in (Figures 15 and 16) demonstrate that for the burner B10, the entrainment zone height decreases as the air Reynolds number increases. This can be stated differently that Figures 15 and 16 reveal that as the primary equivalence ratio, Φ_p, increases the entrainment zone height (the neck height) increases also.

On the other hand, Figure 17 which give the variation of the entrainment zone height with the primary equivalence ratio, Φ_p, at the different number of the fuel ports 12, 24 and 36 indicates that the height of the entrainment zone increases with the increase of the primary equivalence ratios Φ_p, due to the lower rate of momentum exchange at the lower air momentum flux in this case, which results in a decrease of the rate of mixing and the rate of formation of the combustible mixture in the air-fuel boundary layers.

From Figure 17, also it can be concluded that the height of the entrainment zone decreases as the number of the fuel ports increases. This effect is due to the higher momentum exchange at the interfacial surface area of the fuel jets and the central air that is discussed before. This higher momentum exchange completes the fuel jet tangent to the air jet in a shorter height.

On the other hand, if the air jet velocity is low and the fuel jet velocity is also low, the negative pressure developed around both of the air and the fuel jets will be of the same order of magnitude. The drafting of the fuel jets towards the central air jets that takes place due to the existence of the negative pressure gradient in the direction of the central air jet, will not take place. Intermixing between the central air jet and the fuel jets as well as that between the fuel jets and the ambient air will take place due to the interfacial exchange of momentum and mass at much less level than if the velocity of either of the fuel or the air was high. The flame neck ceases to form and the produced flames will take the form of a normal diffusion one. This case is represented by the flame given in Figures 12, which is produced by the continuous decrease of the central air Reynolds number until this diffusion flame was obtained at a central air Reynolds number 2081, fuel Reynolds number 218 and Φp= 4.5 using the three burners B10N12, B10N24 and B10N36 at the same fuel flow rate.

The limiting case is reached when the central air flow ceases, Re_{air}=0 and the resulting flame will categorize that of the self or naturally aspirated diffusion flames.

When the burner B10N36 which has 36 fuel ports was used at the high primary equivalence ratio Φ_p=2 corresponding to the air Reynolds number 4072, the blue color occupied most of the entrainment zone followed by a yellow color which covers a small portion that extends to the neck as shown in Figure 16. The blue color of the entrainment zone produced by the burner of the larger number of the fuel ports B10N36 occupies a larger portion of the flame neck if compared to that encountered in the case of the burners B10N12 and B10N24 at the same primary equivalence ratio Φ_p=2. This is due only to the fact that the circumferential surface area of the larger number of the fuel jets in contact with the air for the 36 fuel jets of the burner B10N36 allowed more local mixing and entrainment of the central air as well as the ambient air in the entrainment zone than in the case of the B10N12

and the 24 fuel jets burners which have less fuel ports.

It is obvious that the early mentioned burner parameters together with the two jets momentum and of course the primary equivalence ratios are the decisive factors that define the nature and the characteristics of the flames from CAP burners.

The study of the influence of these parameters cannot be undertaken collectively, but in determining the effect of any of these parameters, the other parameters must be kept unchanged except of course those parameters which are directly coupled with the parameter under consideration such as the change in the primary equivalence ratio, Φ_p, whenever the air Reynolds number was changed.

Conclusions

1. All the flame characteristics are controlled by the burner geometry and the jet dynamics. For this reason the performance of a port array IDf burner cannot be predicted based on the performance of another burner unless the conditions of the geometric and dynamic similarities are fulfilled.
2. A fuel-air mixture boundary layer is formed at the interfacial surface of the central air-fuel jets after a very short distance from the plane of emergence. In the downstream direction the two jets form a co-flowing jet along the jet path.
3. The fuel jets flowing in the surrounding ambient air form a submerged jet that leads to the formation of another air-fuel mixture boundary layer, called the submerged boundary layer.
4. Two flame fronts are formed in the entrainment zone due to the existence of the two fuel-air mixture boundary layers maintained above.
5. The entrainment zone increases with the decrease of the air Reynolds number. This increase is quite small for the burner which has the small center to center distance, S=10 mm. However it decreases with the increase of the number of the fuel ports.
6. As the number of the fuel ports increases the centerline flame temperature increases provided that the total fuel flow area is kept constant.

Nomenclature

Φ_p: Primary equivalence ratio, dimensionless which is the ratio between the stoichiometric air to fuel ratio to the actual primary, (the central air jet), air to fuel ratio. ($\Phi = \frac{(A/F)_{stoic}}{(A/F)_{Actual}}$).

Φ_o: Overall equivalence ratio, dimensionless which is the ratio between the stoichiometric air to fuel ratio to the summation of the central air jet plus the flow rate of the entrained ambient air to fuel ratio.

d_{air}: The port diameter, mm.
d_{fuel}: The fuel port diameter, mm.
N_f: The number of the fuel ports.
V_{air}: The air velocity, m/s.
V_{fuel}: The fuel velocity, m/s.
Re_{air}: Air jet Reynolds number, dimensionless $(\rho_{air}.v_{air}.d_{air})/\mu_{air}$.
Re_{fuel}: Fuel jet Reynolds number, dimensionless, $(\rho_f.v_f.d_f)/\mu_f$.
ρ_{air}: Air density, kg/m^3.
ρ_{fuel}: Fuel density, kg/m^3.
μ_{air}: The air dynamic viscosity, Pa.s.
μ_{fuel}: The Fuel dynamic viscosity, Pa.s.
Z: Vertical flame distance measured from burner tip, cm.
S: Pitch circle distance, mm.
P: The stagnant ambient air pressure away from the jets.
p_∞: The stagnant pressure of the entrained air at the fuel jet emergence.
Δp: The pressure drop.
R, Radial flame distance.
X_a: Air concentration.
X_f: Fuel concentration.

REFERENCES

Abramovich GN (1963) .The theory of turbulent jets. M.I.T Press. Combride, Massachusetts, translated from Russian by Scripta Techorica, pp. 173-188.

Bradly D, Matthews KJ (1968). Measurement of high gas temperature with fine wire thermocouples. J. Mech. Eng. Sci. 10:299-305.

Choy YS, Zhen HS, Leung CW, Li HB (2012). Pollutant emission and noise radiation from open and impinging inverse diffusion flames. Appl. Energy 91:82–89.

Dong LL, Leung CW (2007). Heat transfer characteristics of an impinging inverse diffusion flame jet – Part I: Free flame structure. Int. J. Heat Mass Transf. 50(25-26):5108–5123.

Elmahalawy F, Habik SE (2002). Fundamentals and technology of combustion. Elsevier.

Huang RF, Yang JT and lee PC (1997). Flame and flow characteristics of double concentric jets. Combust. Flame 108:9-23.

Kline SJ, McClintock FA (1953). Describing uncertainties in single sample experiments. Mech. Eng. 75:3–8.

Lewis B, Pease Rn, Taylor HS (1956). Combustion Processes. Princton University, Press, New Jersey, pp. 386-387.

Mikofski MA, Williams TC, Shaddix CR, Blevins LG (2004). Effect of varied air flow on flame structure of laminar inversed diffusion flame. University of California.

Mikofski MA, Williams TC, Shaddix CR, Fernandez-Pello AC and Blevins LG (2007). Structure of laminar sooting inverse diffusion flames. Combust. Flame 149:463–478.

Patridge WP, Reisel JR, Laurendeau NM (1999). Laser-saturated fluorescence measurements of nitric oxide in an inverse diffusion flame. Combust. Flame 116:282-290.

Salem MR (2007). Analysis of the characteristics of unconfined inversed diffusion flames with circumferentially arranged fuel ports burners. Ain Shams Univ. 42(4):795-821.

Schilichting H (1960). Boundry layer Theory. McGraw-Hill Book Company, New York.

Sze Lip Kit (2007). Thermal and Emission characteristics of an inverse diffusion flame with circumferentially arranged fuel ports. PhD thesis. The Hong Kong Polytechnic University.

Sze LK, Cheung CS, Leung CW (2006). Appearance, temperature and NOx emission of two inverse diffusion flames with different port design. Combust. Flame 144:237-248.

Sze LK, Cheung CS, Leung CW (2004). Temperature distribution and heat transfer characteristics of an inverse diffusion flame with circumferentially arranged ports. Int. J. Heat Mass Transf. 47:3119-3129.

Takagi ZX, Komiyama M (1996). Preferential diffusion effects on the temperature in usual and inverse diffusion flames. Combust. Flame 106:252–260.

Wu KT, Essenhigh RH (1984). Mapping and Structure of Methane. Twentieth Symposium on combustion, pp. 1925-1932.

Zhen HS, Leung CW, Cheung CS (2010). Thermal and emission characteristics of a turbulent swirling inverse diffusion flame. Int. J. Heat Mass Transf. 53:902–909.